Opto-Electronic Advances

Supplementary information

July 2023, Vol. 6, No. 7

DOI: 10.29026/oea.2023.230007

Deep-red and near-infrared organic lasers based on centrosymmetric molecules with excited-state intramolecular double proton transfer activity

Chang-Cun Yan[1,2,3†], Zong-Lu Che[2†], Wan-Ying Yang[2], Xue-Dong Wang[2*] and Liang-Sheng Liao[1,2*]

[1]Macao Institute of Materials Science and Engineering, Macau University of Science and Technology, Taipa, Macau SAR 999078, China; [2]Institute of Functional Nano & Soft Materials, Jiangsu Key Laboratory for Carbon-Based Functional Materials & Devices, Joint International Research Laboratory of Carbon-Based Functional Materials and Devices, Soochow University, Suzhou 215123, China; [3]Jiangsu Engineering Laboratory of Novel Functional Polymeric Materials, Jiangsu Key Laboratory of Advanced Negative Carbon Technologies, College of Chemistry, Chemical Engineering and Materials Science, Soochow University, Suzhou 215123, China.

†These authors contributed equally to this work.

*Correspondence: XD Wang, E-mail: wangxuedong@suda.edu.cn; LS Liao, E-mail: lsliao@suda.edu.cn

This file includes:

Supplementary information for this paper is available at https://doi.org/10.29026/oea.2023.230007

Section 1: Synthesis of Gain Materials

General Information

All the reactants and reagents were commercially available and used as received unless otherwise stated. THF was purified by PURE SOLV (Innovative Technology) purification system. All reactions were monitored by thin layer chromatography (TLC). Column chromatography was performed over silica gel (200-300 mesh). NMR were measured in $CDCl_3$ solutions by a Bruker AVANCEIII HD-400 NMR spectrometer at 298K with the internal standard of tetramethylsilane (TMS). Chemical shifts (δ) are recorded in parts per million (ppm) and coupling constants (J) are reported in Hertz (Hz).

Synthetic Route

(*E*)-3-(4-(dimethylamino)phenyl)-1-(2-hydroxyphenyl)prop-2-en-1-one (**HPMP**), (*E*)-3-(4-(diphenylamino)phenyl)-1-(2-hydroxyphenyl)prop-2-en-1-one (**HPPP**) and (*E*)-1-(2-hydroxyphenyl)-3-(2,3,6,7-tetrahydro-1H,5H-pyrido[3,2,1-ij]quinolin-9-yl)prop-2-en-1-one (**HPJP**) were synthesized according to previously reported method (Scheme S1)[S1].

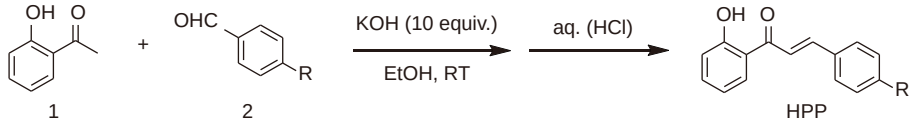

Scheme S1 | Sythetic route of HPMP, HPPP and HPJP.

(2*E*,2'*E*)-1,1'-(1,5-dimethoxynaphthalene-2,6-diyl)bis(3-(4-(dimethylamino)phenyl)prop-2-en-1-one) (**DMN-DMP**), (2*E*,2'*E*)-1,1'-(1,5-dimethoxynaphthalene-2,6-diyl)bis(3-(4-(diphenylamino)phenyl)prop-2-en-1-one) (**DMN-DPP**), (2*E*,2'*E*)-1,1'-(1,5-dimethoxynaphthalene-2,6-diyl)bis(3-(2,3,6,7-tetrahydro-1H,5H-pyrido[3,2,1-ij]quinolin-9-yl)prop-2-en-1-one) (**DMN-DJP**), (2*E*,2'*E*)-1,1'-(1,5-dihydroxynaphthalene-2,6-diyl)bis(3-(4-(dimethylamino)phenyl)prop-2-en-1-one) (**DHN-DMP**), (2*E*,2'*E*)-1,1'-(1,5-dihydroxynaphthalene-2,6-diyl)bis(3-(4-(diphenylamino)phenyl)prop-2-en-1-one) (**DHN-DPP**) and (2*E*,2'*E*)-1,1'-(1,5-dihydroxynaphthalene-2,6-diyl)bis(3-(2,3,6,7-tetrahydro-1H,5H-pyrido[3,2,1-ij]quinolin-9-yl)prop-2-en-1-one) (**DHN-DJP**) were synthesized according to the synthetic route as shown in Scheme S2. Compound **3** was synthesized according to previously reported work[S2].

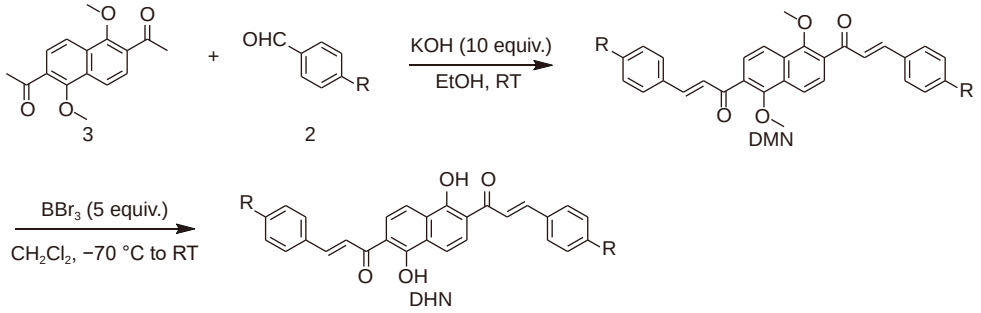

Scheme S2 | The synthetic route of DMNs and DHNs.

General method for the synthesis of **DMN**s.

In a 100 mL round-bottomed flask, a mixture of a mixture of compound **3** (1.0 mmol) and KOH (10 mmol) was dissolved in ethanol (10 mL). After stirring at room temperature for 1 h, compound **2** (2.0 mmol) was added. After stirring at room temperature for another 10 h, the resulting mixture was poured into 100 mL water to give an orange precipitate. The solid was filtered, washed with H_2O (2 × 10 mL), dried under vacuum at 50 °C for 24 h. The result crude product was subjected to silica gel flash chromatography, and the concentration of the appropriate fractions in vacuo afforded **DMN**.

General method for the synthesis of **DHN**s.

A solution of **DMN** (0.5 mmol) in CH_2Cl_2 (50 mL) was treated at −78 °C dropwise with BBr_3 (1.0 M in CH_2Cl_2, 2.5 mL, 2.5 mmol) over 10 min and stirred for 1 h. The reaction mixture was quenched with saturated aq. $NaHCO_3$ (20

mL). The organic layer was separated and washed with H_2O (3 × 20 mL) and brine (20 mL), dried with anhydrous Na_2SO_4, filtered and concentrated under reduced pressure. The result crude product was subjected to silica gel flash chromatography, and the concentration of the appropriate fractions in vacuo afforded **ADH**.

Characterizations

HPJP:

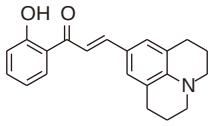

Dark-red solid, yield: 83%.

^{1}H NMR (400 MHz, $CDCl_3$) δ 13.31 (s, 1H), 7.93 (dd, J = 8.0, 1.6 Hz, 1H), 7.84 (d, J = 15.2 Hz, 1H), 7.44 (ddd, J = 8.4, 7.2, 1.6 Hz, 1H), 7.38 (d, J = 15.2 Hz, 1H), 7.14 (s, 2H), 6.99 (dd, J = 8.4, 1.2 Hz, 1H), 6.90 (ddd, J = 8.4, 7.2, 1.2 Hz, 1H), 3.27 (t, J = 6.0 Hz, 4H), 2.77 (t, J = 6.4 Hz, 4H), 2.03–1.92 (m, 4H).

^{13}C NMR (100 MHz, $CDCl_3$) δ 193.28, 163.48, 147.04, 145.76, 135.39, 129.29, 128.64, 121.32, 121.04, 120.56, 118.46, 118.44, 112.99, 50.01, 27.71, 21.49.

IR (cm^{-1}) 3017, 2970, 2940, 2911, 2843, 1738, 1624, 1541, 1508, 1481, 1437, 1366, 1304, 1240, 1196, 1148, 1026, 976, 833, 814, 764, 658.

HRMS (ESI) m/z: $[M+H]^+$ calculated for $C_{21}H_{22}NO_2^+$, 320.1645; found 320.1628.

DMN-DMP:

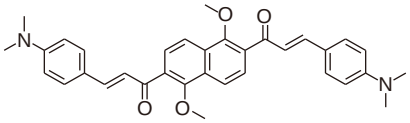

Orange-red solid, yield: 79%.

^{1}H NMR (400 MHz, $CDCl_3$) δ 8.07 (d, J = 8.4 Hz, 2H), 7.73 (d, J = 8.4 Hz, 2H), 7.68 (d, J = 15.6 Hz, 2H), 7.54 (d, J = 8.8 Hz, 4H), 7.34 (d, J = 15.6 Hz, 2H), 6.69 (d, J = 8.8 Hz, 4H), 3.97 (s, 6H), 3.05 (s, 12H).

^{13}C NMR (100 MHz, $CDCl_3$) δ 193.37, 155.83, 152.15, 146.29, 130.98, 130.62, 130.36, 126.73, 122.48, 121.40, 118.85, 111.85, 63.84, 40.13.

IR (cm^{-1}) 2996, 2970, 2947, 1738, 1593, 1524, 1437, 1370, 1227, 1217, 1184, 1134, 1018, 980, 804, 675, 623.

HRMS (ESI) m/z: $[M+H]^+$ calculated for $C_{34}H_{35}N_2O_4^+$, 535.2591; found 535.2581.

DMN-DPP:

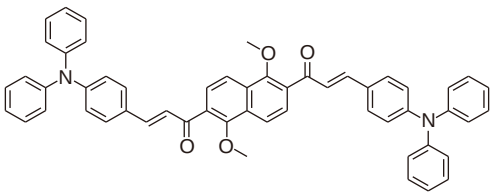

Orange-red solid, yield: 81%.

^{1}H NMR (400 MHz, $CDCl_3$) δ 8.06 (d, J = 8.4 Hz, 2H), 7.74 (d, J = 8.4 Hz, 2H), 7.67 (d, J = 16.0 Hz, 2H), 7.47 (d, J = 8.8 Hz, 4H), 7.40 (d, J = 16.0 Hz, 2H), 7.30 (td, J = 7.2, 2.0 Hz, 8H), 7.17–7.07 (m, 12H), 7.02 (d, J = 8.8 Hz, 4H), 3.96 (s, 6H).

^{13}C NMR (100 MHz, $CDCl_3$) δ 193.15, 156.19, 150.34, 146.76, 144.96, 131.15, 130.18, 129.92, 129.53, 127.60, 126.72, 125.54, 124.22, 123.67, 121.44, 119.01, 64.00.

IR (cm^{-1}) 3026, 2970, 2943, 1740, 1580, 1483, 1371, 1350, 1267, 1217, 1065, 1032, 980, 820, 752, 694, 619.

HRMS (ESI) *m*/*z*: [M+H]$^+$ calculated for $C_{54}H_{43}N_2O_4^+$, 783.3217; found 783.3198.

DMN-DJP:

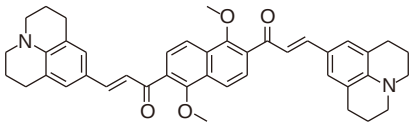

Orange-red solid, yield: 75%.

^{1}H NMR (400 MHz, $CDCl_3$) δ 8.04 (d, J = 8.4 Hz, 2H), 7.69 (d, J = 8.4 Hz, 2H), 7.58 (d, J = 15.6 Hz, 2H), 7.24 (d, J = 15.6 Hz, 2H), 7.09 (s, 4H), 3.95 (s, 6H), 3.25 (t, J = 5.6 Hz, 8H), 2.74 (t, J = 6.4 Hz, 9H), 2.01–1.90 (m, 8H).

^{13}C NMR (100 MHz, $CDCl_3$) δ 193.33, 155.60, 146.89, 145.42, 130.85, 130.47, 128.38, 126.78, 121.38, 121.05, 120.29, 118.74, 63.72, 49.98, 27.69, 21.54.

IR (cm^{-1}) 3015, 2970, 2928, 2839, 1738, 1643, 1546, 1510, 1435, 1371, 1314, 1204, 1161, 1065, 1028, 1009, 831, 812, 737, 689.

HRMS (ESI) *m*/*z*: [M+H]$^+$ calculated for $C_{42}H_{43}N_2O_4^+$, 639.3217; found 639.3210.

DHN-DMP:

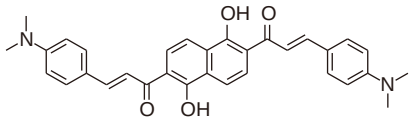

Dark-red solid, yield: 56%.

^{1}H NMR (400 MHz, $CDCl_3$) δ 14.94 (s, 2H), 8.03 (d, J = 15.2 Hz, 2H), 7.96 (d, J = 15.2 Hz, 2H), 7.65 (d, J = 8.8 Hz, 4H), 7.60 (d, J = 14.8 Hz, 2H), 7.31 (d, J = 14.8 Hz, 2H), 6.75 (d, J = 8.8 Hz, 4H), 3.11 (s, 12H).

IR (cm^{-1}) 3015, 2970, 2945, 2922, 2807, 1738, 1605, 1545, 1520, 1429, 1364, 1217, 1188, 1115, 974, 945, 903, 804, 698.

HRMS (ESI) *m*/*z*: [M+H]$^+$ calculated for $C_{32}H_{31}N_2O_4^+$, 507.2278; found 507.2271.

DHN-DPP:

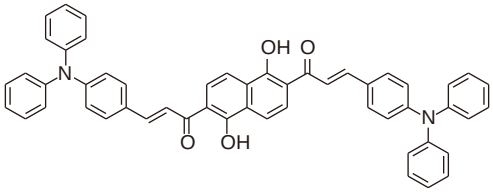

Dark-red solid, yield: 79%.

^{1}H NMR (400 MHz, $CDCl_3$) δ 14.72 (s, 2H), 7.97 (d, J = 15.2 Hz, 2H), 7.94 (d, J = 8.4 Hz, 2H), 7.91 (d, J = 8.4 Hz, 2H), 7.62 (d, J = 15.2 Hz, 2H), 7.56 (d, J = 8.8 Hz, 4H), 7.36–7.29 (m, 8H), 7.20–7.11 (m, 12H), 7.05 (d, J = 8.8 Hz, 4H).

IR (cm^{-1}) 3015, 2970, 2947, 1738, 1553, 1485, 1427, 1366, 1271, 1217, 1173, 1117, 974, 806, 754, 694, 617.

HRMS (ESI) *m*/*z*: [M+H]$^+$ calculated for $C_{52}H_{39}N_2O_4^+$, 755.2904; found 755.2875.

DHN-DJP:

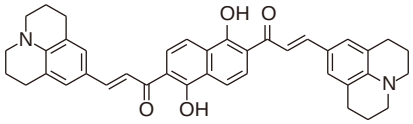

Dark-red solid, yield: 61%.

^{1}H NMR (400 MHz, $CDCl_3$) δ 15.09 (s, 2H), 7.99–7.90 (m, 6H), 7.51 (d, J = 15.2 Hz, 2H), 7.21 (s, 4H), 3.31 (t, J = 5.6

Hz, 8H), 2.82 (t, J = 6.4 Hz, 8H), 2.07–1.96 (m, 8H).

IR (cm^{-1}) 3015, 2970, 2938, 2839, 1738, 1589, 1537, 1506, 1427, 1371, 1298, 1230, 1217, 1198, 1159, 1113, 1072, 1049, 974, 889, 835, 799, 729, 694.

HRMS (ESI) m/z: $[M+H]^+$ calculated for $C_{40}H_{39}N_2O_4^+$, 611.2904; found 611.2891.

Section 2: Single crystal information

The crystal was obtained by slow evaporation of CH_2Cl_2/EtOH. Single-crystal XRD data were collected on a Bruker D8-Venture diffractometer with a Turbo X-ray Source (Mo-Kα radiation, λ = 0.71073 A), adopting the direct drive rotating anode technique and a CMOS detector at room temperature. The data frames were collected using the APEX2 program and processed using the program SAINT routine in APEX2. Structures were solved by direct methods and refined by the full-matrix least squares on F2 using the SHELXTL-2014 program. Crystallographic data were compared with the Cambridge Crystallographic Data Center supplementary publication no. CCDC-2081135 (DHN-DMP), no. CCDC-2236316 (DHN-DPP) and no. CCDC-2236314 (DHN-DJP).

Section 3: Theoretical calculations

All density functional theory (DFT) calculations were performed by the Gaussian 16 program[S3]. The structures and energies were calculated at (TD)-wB97xD/6–31+G(d,p) level[S4–S7]. Imaginary frequencies were examined for all transition states. The Gibbs free energies were obtained from the frequency calculations.

Section 4: Fabrication and characterization of PS films and microspheres

The fabrication of small molecule-doped PS films and microspheres is according to previously reported procedures[S8].

Preparation of PS films

PS films were prepared by drop-casting from **DHN**/PS/DCM solution. First, an amount of **DHN** and 10.0 mg of PS were dissolved in 1 mL of DCM under stirring. Then, the solution was drop-cast onto quartz wafers in air. After total evaporation of CH_2Cl_2, **DHN**:PS films (124 ± 9 μm) were obtained.

PS blend films with thicknesses range from 800 nm to 3 μm were prepared by spin-coating the **DHN**/PS/$CHCl_3$ solution on quartz wafers in air, followed by a 5-min annealing at 100 °C. The thicknesses of the films were controlled by the rotational speed during spin-coating.

Preparation of PS microspheres

DHN-doped microspheres were prepared through an emulsion-solvent evaporation method. In a typical preparation, 200 μL of well-mixed **DHN**/PS/DCM solution (0.5 mg/mL **DHN** and 50.0 mg/mL PS) was added to 2.0 mL of **CTAB** aqueous solution (1.0 mg/mL), which was subsequently treated with vigorous stirring. After aging for 2 h, the DCM was completely evaporated, and **DHN**-doped microspheres were obtained and dispersed in the colloid solution. The surfactant **CTAB** was removed by filtration and washing. The precipitate was redispersed in the aqueous solution and used to prepare samples for further characterization by drop-casting. The diameter of the obtained sphere can be well controlled by changing the concentration of PS.

Same methods were adopted in the preparation of other compounds doped PS films and microspheres.

Characterizations of well-prepared PS microspheres

Microscopy images were obtained using a Leica DMRBE fluorescence microscope with a spot-enhanced charge couple device (CCD, Diagnostic Instrument, Inc.). Field-emission scanning electron microscopy (FESEM) image of the samples were observed using an FESEM (Carl Zeiss, Supra 55).

Section 5: Optical characterizations

Ultraviolet-visible absorption spectra were measured by a Shimadzu UV-2600 spectrophotometer. Photoluminescence spectra were measured by a Horiba JY FL-3 fluorescence spectrophotometer (NIR-VIS, FL3). Absolute PL quantum yields (PLQY) were measured on a Quantaurus-QY measurement system (C11347-11, Hamamatsu Photonics). The transient PL decay characteristics were recorded using a Quantaurus-Tau fluorescence lifetime measurement system

(C11367-03, Hamamatsu Photonics).

A homemade micro-photoluminescence (μ-PL) system (Fig. S12) was used to measure μ-PL spectra. The samples were excited by a 532 nm pump laser (repetition rate = 10 Hz; pulse duration = 10 ns) passing a 532 nm notch filter. The minimum diameter of light spot is 50 μm and the size is adjustable. Then, the fluorescence from samples was collected into a grating spectrometer (Princeton Instrument, ARC-SP-2356) and detected by a thermal-electrically cooled CCD (Princeton Instruments, PIX-256E). Microscopy images were taken with an inverted microscope (Olympus, BX43).

Section 6: Supporting Figures

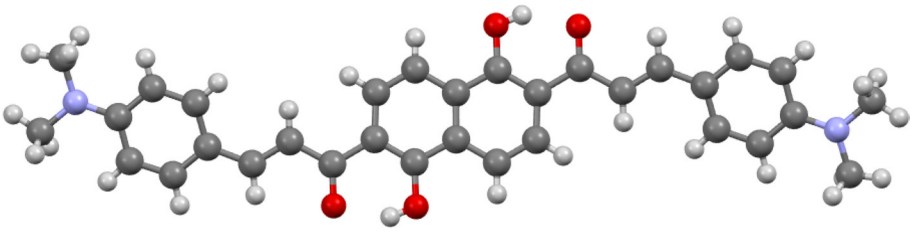

Fig. S1 | Single crystal structure of DHN-DMP.

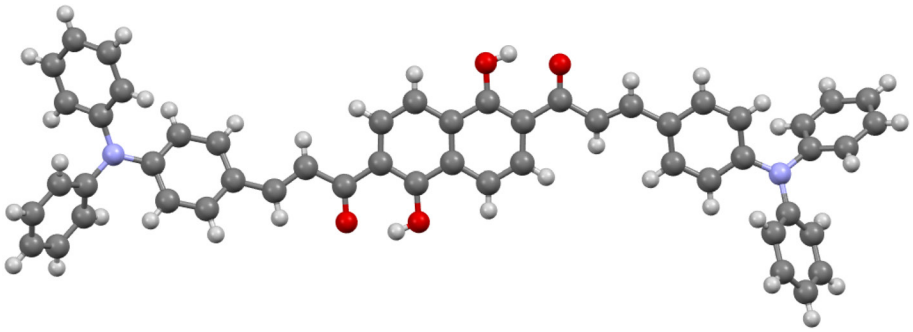

Fig. S2 | Single crystal structure of DHN-DPP.

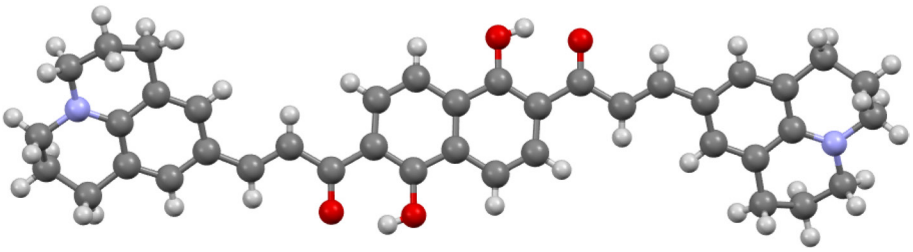

Fig. S3 | Single crystal structure of DHN-DJP.

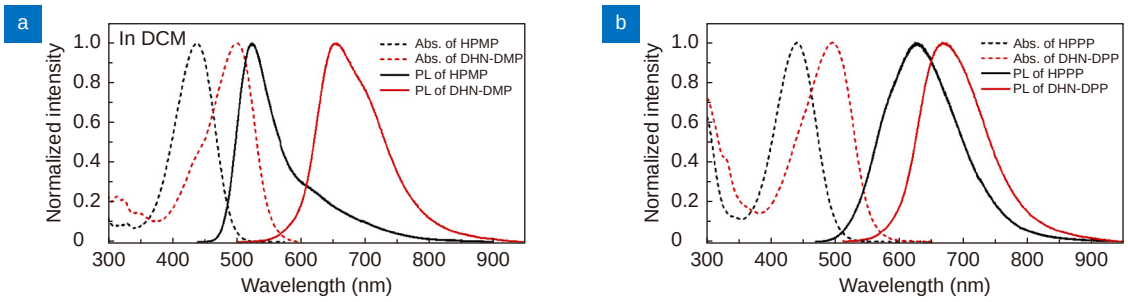

Fig. S4 | (**a**) The UV-vis absorption and PL spectra of HPMP and DHN-DMP in DCM solutions. (**b**) The UV-vis absorption and PL spectra of HPPP and DHN-DPP in DCM solutions.

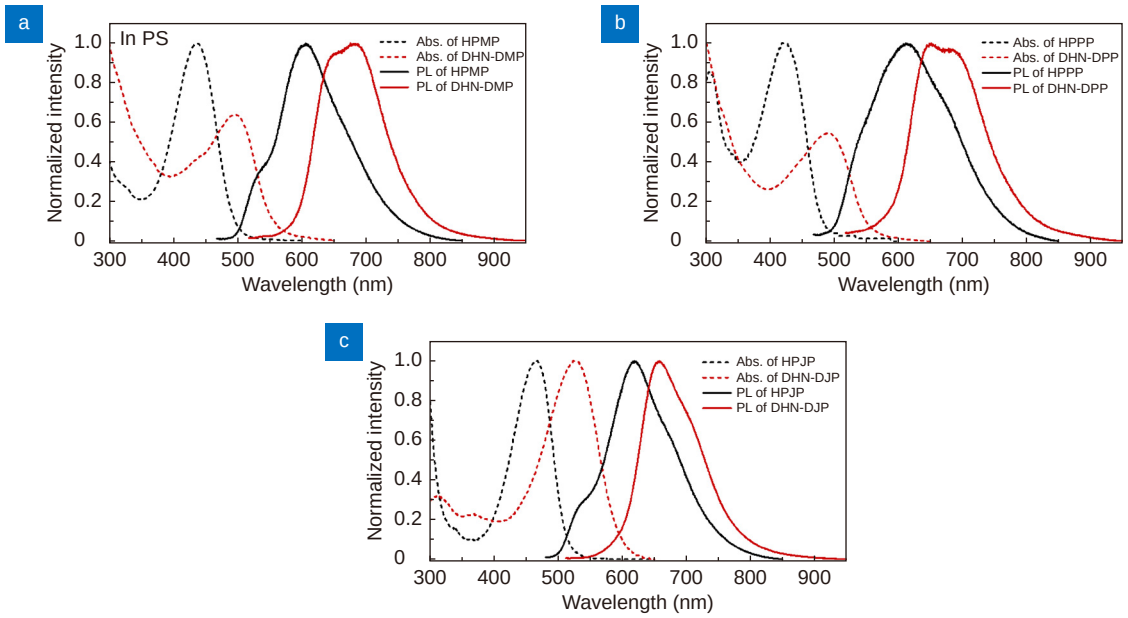

Fig. S5 | (**a**) The UV-vis absorption and PL spectra of HPMP and DHN-DMP in PS films. (**b**) The UV-vis absorption and PL spectra of HPPP and DHN-DPP in PS films. (**c**) The UV-vis absorption and PL spectra of HPJP and DHN-DJP in PS films.

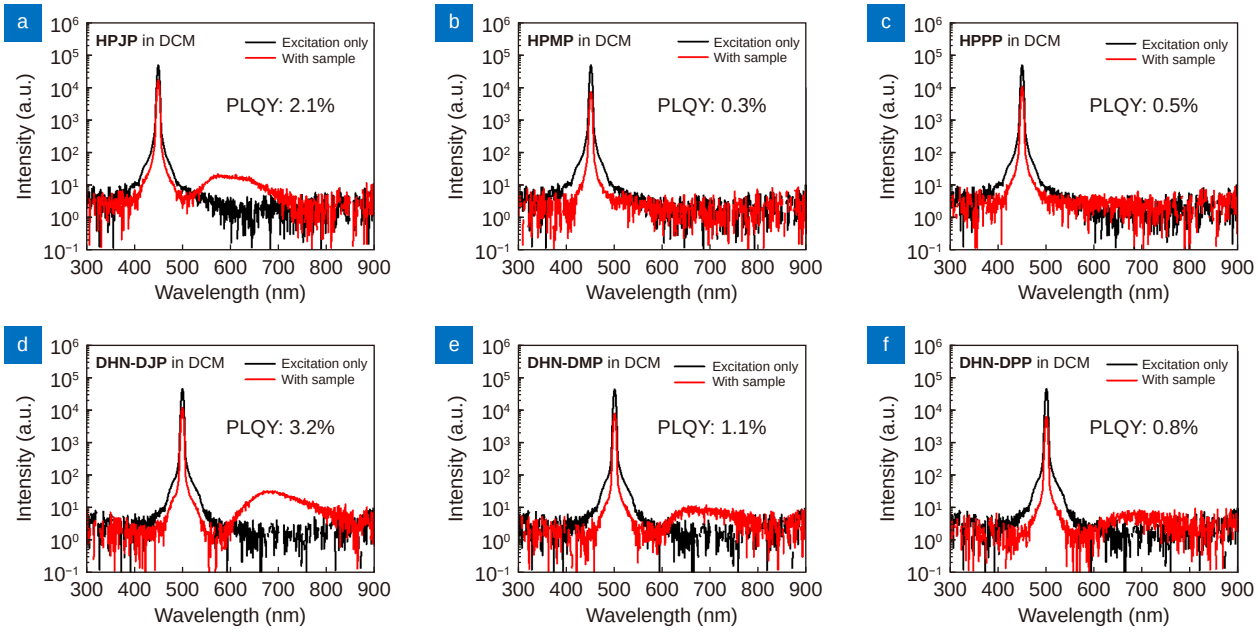

Fig. S6 | Emission spectra for PLQY measurements in DCM.

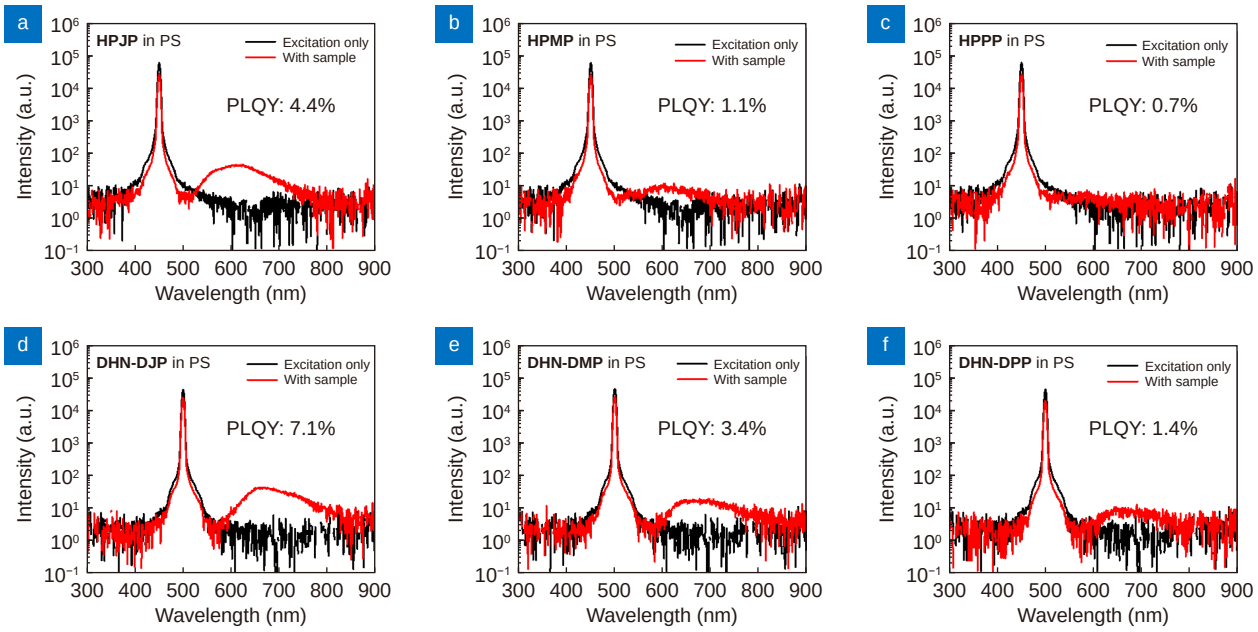

Fig. S7 | Emission spectra for PLQY measurements in PS films.

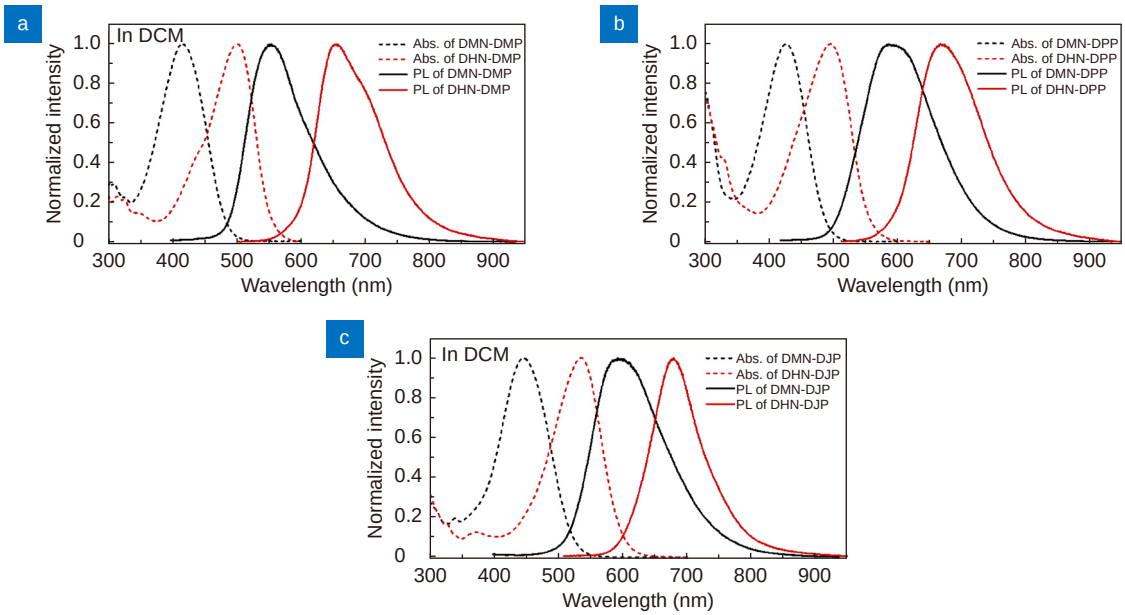

Fig. S8 | (**a**) The UV-vis absorption and PL spectra of DMN-DMP and DHN-DMP in DCM solutions. (**b**) The UV-vis absorption and PL spectra of DMN-DPP and DHN-DPP in DCM solutions. (**c**) The UV-vis absorption and PL spectra of DMN-DJP and DHN-DJP in DCM solutions.

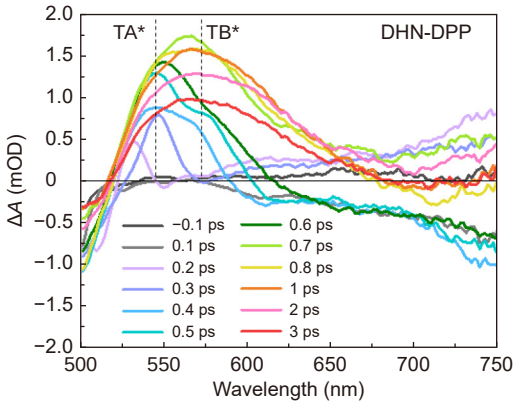

Fig. S9 | The transient spectral profiles of DHN-DPP in polystyrene.

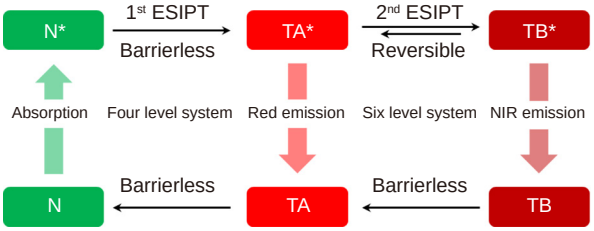

Fig. S10 | Diagram of ESIPT processes of DHNs.

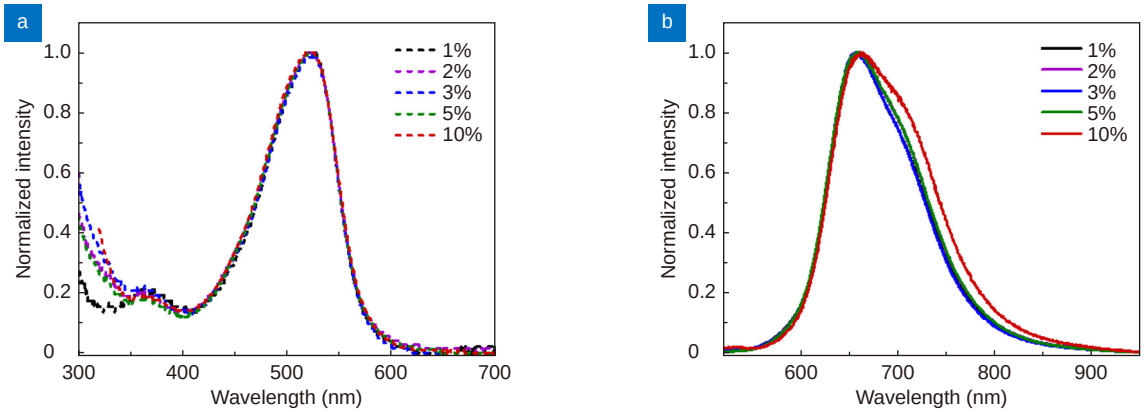

Fig. S11 | The (**a**) UV-vis absorption and (**b**) PL spectra of DHN-DJP in PS films with different doping concentration.

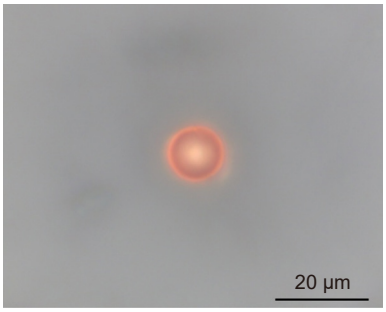

Fig. S12 | The bright-field image of a selected single microsphere.

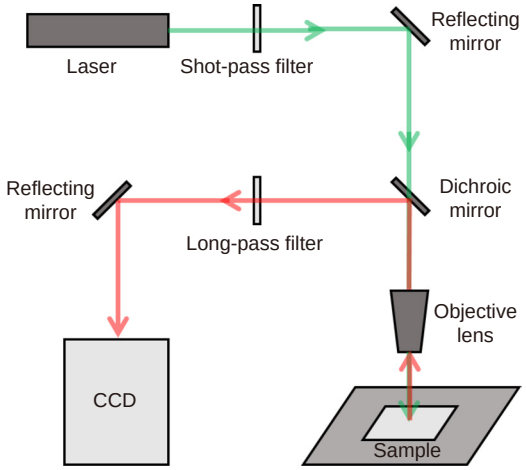

Fig. S13 | The diagram of the setup of the home-made μ-PL system.

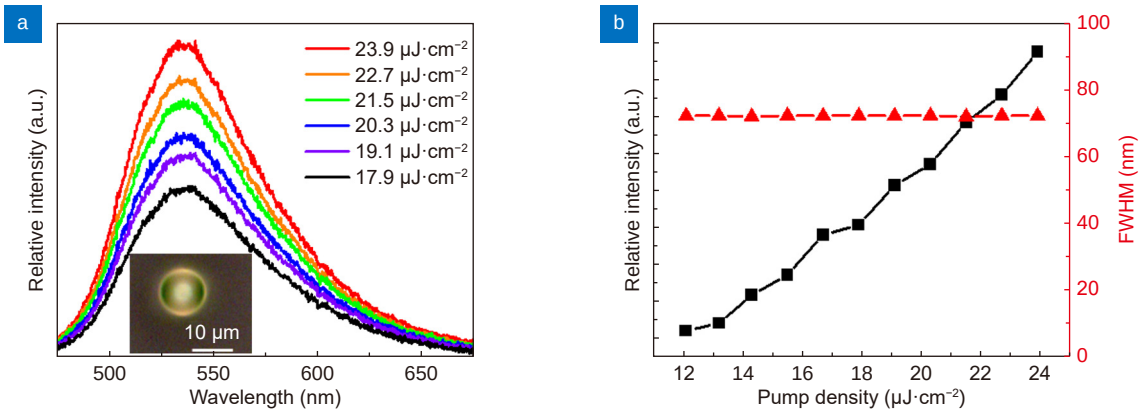

Fig. S14 | (**a**) PL spectra of a DMN-DJP doped PS microsphere under different pump density. Inset: brightfield micrograph of the microsphere used in the laser measurement. (**b**) Plots of lasing intensity (black blocks) and full width at half-maximum (FWHM, red triangles) as a function of pump density.

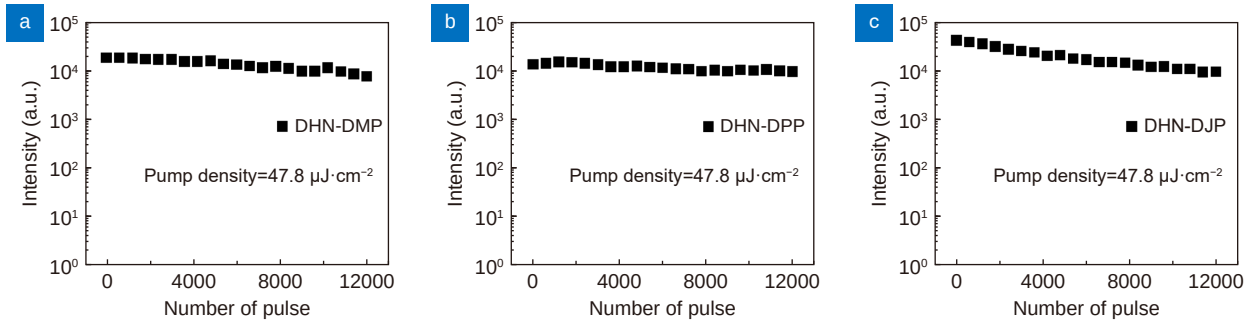

Fig. S15 | Plots of lasing intensity (black blocks) as a function of number of pulses.

Section 7: Supporting Tables

Table S1 | The summary of the parameters of DHN-DMP unit cell.

Formula	$C_{32}H_{30}N_2O_4$
Formula weight	506.58
Crystal system	triclinic
Space group	P −1
a (Å)	5.1154(4)
b (Å)	11.8779(9)
c (Å)	12.1137(10)
α (°)	116.915(4)
β (°)	102.128(2)
γ (°)	92.562(3)
V (Å)	633.35
Cell formula units, *Z*, *Z′*	*Z*: 1, *Z′*: 0.5
R factor (%)	5.23

Table S2 | The summary of the parameters of DHN-DPP unit cell.

Formula	$C_{52}H_{38}N_2O_4$
Formula weight	924.69
Crystal system	triclinic
Space group	P −1
a (Å)	9.6001(2)
b (Å)	10.5402(3)
c (Å)	23.3855(6)
α (°)	102.7450(10)
β (°)	92.9740(10)
γ (°)	101.5650(10)
V (Å)	2249.68
Cell formula units, *Z*, *Z′*	*Z*: 2, *Z′*: 1
R factor (%)	7.14

Table S3 | The summary of the parameters of DHN-DJP unit cell.

Formula	$C_{40}H_{38}N_2O_4$
Formula weight	610.72
Crystal system	monoclinic
Space group	P 2_1/c
a (Å)	8.4182(2)
b (Å)	11.1467(3)
c (Å)	15.8142(4)
α (°)	90
β (°)	95.282(2)
γ (°)	90
V (Å)	1477.63
Cell formula units, *Z*, *Z′*	*Z*: 2, *Z′*: 0.5
R factor (%)	4.89

Table S4 | Statistics analyses of the fitting curves of decay plots of DHNs in Figure 3.

	Reduced Chi square	Residual sum of square	R-square (COD)
DHN-DMP at 650 nm	7.4290E–6	0.0126	0.9992
DHN-DMP at 685 nm	6.9301E–6	0.0117	0.9989
DHN-DPP at 650 nm	5.5653E–6	0.0094	0.9991
DHN-DPP at 685 nm	7.1847E–6	0.0122	0.9970
DHN-DJP at 650 nm	9.0527E–6	0.0066	0.9991
DHN-DJP at 710 nm	5.6521E–6	0.0097	0.9987

References

S1. Cheng X, Wang K, Huang S, Zhang HY, Zhang HY et al. Organic crystals with near-infrared amplified spontaneous emissions based on 2'-hydroxychalcone derivatives: subtle structure modification but great property change. *Angew Chem Int Ed* **54**, 8369–8373 (2015).

S2. Yan CC, Wu JJ, Yang WY, Chen S, Lv Q et al. Precise synthesis of multilevel branched organic microwires for optical signal processing in the near infrared region. *Sci China Mater* **65**, 1020–1027 (2022).

S3. Frisch MJ, Trucks GW, Schlegel HB, Scuseria GE, Robb MA et al. *Gaussian 16* (Gaussian, Inc. , Wallingford, 2016).

S4. Chai JD, Head-Gordon M. Long-range corrected hybrid density Functionals with damped atom–atom dispersion corrections. *Phys Chem Chem Phys* **10**, 6615–6620 (2008).

S5. McLean AD, Chandler GS. Contracted Gaussian basis sets for molecular calculations. I. Second row atoms, Z=11–18. *J Chem Phys* **72**, 5639–5648 (1980).

S6. Frisch MJ, Pople JA, Binkley JS. Self‐consistent molecular orbital methods 25. Supplementary functions for Gaussian basis sets. *J Chem Phys* **80**, 3265–3269 (1984).

S7. Marucho M, Pettitt BM. Optimized theory for simple and molecular fluids. *J Chem Phys* **126**, 124107 (2007).

S8. Yan CC, Liu YP, Yang WY, Wu JJ, Wang XD et al. Excited-state intramolecular proton transfer parent core engineering for six-level system lasing toward 900 nm. *Angew Chem Int Ed* **61**, e202210422 (2022).